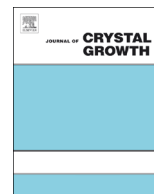




ELSEVIER

Contents lists available at ScienceDirect

Journal of Crystal Growth

journal homepage: www.elsevier.com/locate/jcrysgr

GaN films and GaN/AlGaIn quantum wells grown by plasma assisted molecular beam epitaxy using a high density radical source



Yvon Cordier^{a,*}, Benjamin Damilano^a, Phannara Aing^b, Catherine Chaix^b, Florence Linez^c, Filip Tuomisto^c, Philippe Vennéguès^a, Eric Frayssinet^a, Denis Lefebvre^a, Marc Portail^a, Maud Nemoz^a

^a CRHEA, CNRS UPR 10, rue Bernard Grégory, 06560 Valbonne, France

^b RIBER SA, 31 rue Casimir Perier, 95873, Bezons, France

^c Department of Applied Physics, Aalto University, P.O. Box 14100, FI-00076 Aalto, Finland

ARTICLE INFO

Article history:

Received 12 June 2015

Received in revised form

6 October 2015

Accepted 19 October 2015

Communicated by: E. Calleja

Available online 27 October 2015

Keywords:

A1. Crystal morphology

A1. Impurities

A1. Point defects

A3. Molecular beam epitaxy

A3. Quantum wells

B1. Nitrides

ABSTRACT

The behavior of a high density radical source for the plasma assisted molecular beam epitaxy of GaN and AlGaIn compounds is studied and compared with the one of a conventional plasma source. Plasma light emission correlates with the GaN growth rate. Both attest to the better efficiency of the new source for producing active nitrogen species with resulting growth rates well beyond 1 $\mu\text{m}/\text{h}$. The present study shows that GaN films with equivalent structural and optical quality can be grown even with a growth rate enhancement by a factor of 5. The purity of the grown films is investigated as well as point defects. Positron annihilation shows that plasma conditions can be tuned in order to limit the increase of the gallium-vacancy related complexes density by about $2 \times 10^{16} \text{ cm}^{-3}$ while reaching growth rates as high as 2.1 $\mu\text{m}/\text{h}$.

© 2015 Elsevier B.V. All rights reserved.

1. Introduction

For a long time, the plasma assisted molecular beam epitaxy (PAMBE) growth of III-Nitride materials has been impeded by the weak efficiency of the nitrogen plasma sources and their resulting low growth rate (typically below 0.5 $\mu\text{m}/\text{h}$ for GaN) compared to ammonia source MBE (typically 0.5–1 $\mu\text{m}/\text{h}$) and metal organic vapor phase epitaxy (MOVPE) with typical growth rate of 2 $\mu\text{m}/\text{h}$. This can be a severe limitation for production. To solve this limitation, the use of several nitrogen plasma sources within the same reactor [1] has been proposed as well as new types of plasma sources [2,3]. Among these sources the high density radical source (HDRS) has been co-developed by the University of Nagoya and the company NU EcoEngineering Co. [2,4]. The nitrogen radicals are supplied by conventional plasma sources with the application of RF power into a BN cavity containing the nitrogen flow. One approach to achieve high density nitrogen radicals and then higher growth rate is to increase the plasma densities. As described in [4], this can be achieved within inductively coupled plasma

(ICP). Thanks to the enhancement of the efficiency, not only a higher growth rate is expected, but also for a given growth rate, a reduced RF power to generate active species which in return can benefit to the quality of materials like GaN, AlGaIn and InGaIn [4]. In the present work, we evaluate the capabilities of such a HDRS for the PAMBE growth of GaN films as well as for GaN/AlGaIn quantum well structures. Comparisons with films grown with NH_3 MBE are also made.

2. Experimental methods

Epilayers are grown in a RIBER Compact 21T molecular beam epitaxy reactor dedicated to the growth of III-nitrides. Previously, this reactor has been evaluated for the growth of GaN based structures using ammonia thermally cracked at the sample surface [5–7] and PAMBE with a conventional source (CS) from RIBER/ADDON [7–9]. GaN and AlGaIn films are grown on 3–4 μm GaN-on-sapphire MOVPE templates with a 1 μm thick Mo coating on the backside to facilitate heating as well as temperature measurements with an infrared pyrometer. GaN films are also grown on 3 in. diameter AlN/Si(111) templates in order to assess the

* Corresponding author.

E-mail address: yc@crhea.cnrs.fr (Y. Cordier).

uniformity with Fourier transform infrared (FTIR) spectroscopy as described in [10]. The growth temperature is set to 720 °C. In order to obtain the best material quality, the chosen growth conditions are slightly Gallium rich and are monitored using reflection high energy electron diffraction (RHEED). While a Gallium beam equivalent pressure (BEP) of less than 9×10^{-7} Torr is sufficient to grow GaN at 0.5 $\mu\text{m}/\text{h}$, the flux has to be increased to reach high growth rates accordingly. For this reason, two Gallium effusion cells equipped with pyrolytic graphite crucibles (RIBER MS440) are used when growth operates at rates superior to 1 $\mu\text{m}/\text{h}$. For Aluminum, a Cold Neck effusion cell with a pyrolytic Boron Nitride crucible is used (RIBER ABN60/80CN). The cryopanel cooling with liquid nitrogen has much less influence on the growth pressure when using nitrogen plasma instead of NH_3 . In the present case, the turbo pump can absorb 2400 l/s of nitrogen. The pressure in the reactor increases linearly with the nitrogen flow rate and reaches 3.5×10^{-5} Torr for the maximum flow rate of 10 sccm. Like the CS, the HDRS cell is equipped with a viewport in order to collect the infrared light emitted by the plasma. The optical sensor developed by RIBER operates in the wavelength range of 750–850 nm and produces an output voltage as a direct measurement of the amount of active nitrogen available for growth [11]. The growth rate is measured in-situ with a laser reflectivity set-up (637 nm wavelength laser beam). In the present configuration, the period of the reflectivity signal oscillations is 133 nm for GaN as confirmed by thickness measurements made using cross section scanning electron microscopy.

The surface of the different grown samples is inspected using tapping mode atomic force microscopy (AFM) [11]. A Panalytical crystal X-ray diffractometer using $\text{CuK}\alpha$ radiation is employed to evaluate the Al molar fraction in AlGaIn alloys. The GaN/AlGaIn QW crystal quality is also investigated using cross-section transmission electron microscopy (TEM) in a JEOL 2010F microscope operating at 200 kV. The optical properties are assessed by photoluminescence using the 244 nm line of a frequency doubled Ar laser at room temperature, and in some cases at low temperature (14 K) in a closed cycle optical cryostat. Secondary ion mass spectrometry (SIMS) is used to evaluate the impurities concentrations in the grown films. A Mercury probe set-up is used to perform capacitance–voltage (CV) measurements without device processing in order to assess the residual active donor density in the grown films. Moreover, positron annihilation spectroscopy [12] is carried out in order to assess the layers quality in terms of point defects. As shown below we first detail the growth rate of GaN films using different nitrogen flow rates and RF powers before assessing the quality of the grown structures.

3. Results and discussion

3.1. Growth rates

The effect of the nitrogen flow rate and RF power on the growth rate of GaN films is reported in Fig. 1. Our previous results obtained with a conventional source [7] are reported in the figure for comparison. It is obvious here that the efficiency of the HDRS is much better. For instance, the growth rate is enhanced from 0.4 $\mu\text{m}/\text{h}$ with the CS to more than 0.8 $\mu\text{m}/\text{h}$ with HDRS using the same RF power of 400 W and N_2 flow rates of 1.8–2 sccm. More, the growth rate can be increased beyond 2 $\mu\text{m}/\text{h}$ while increasing the N_2 flow rate (7–9 sccm) and the power (400–500 W) and no drop of the GaN growth rate is observed at high N_2 flow rates contrary to what is observed with the CS [11] for similar experimental conditions. The intensity of the light emitted by the plasma is reported in Fig. 2. The dependence with the nitrogen flow rate and the RF power is very similar to the one of the growth rate and

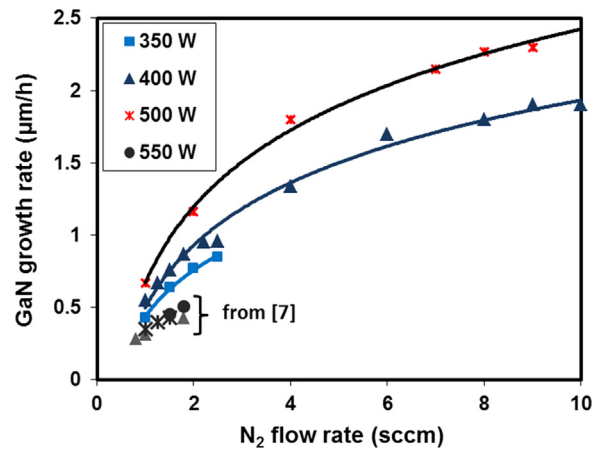


Fig. 1. GaN growth rate as a function of N_2 flow rate and HDRS RF power. Data from [7] have been added for comparisons.

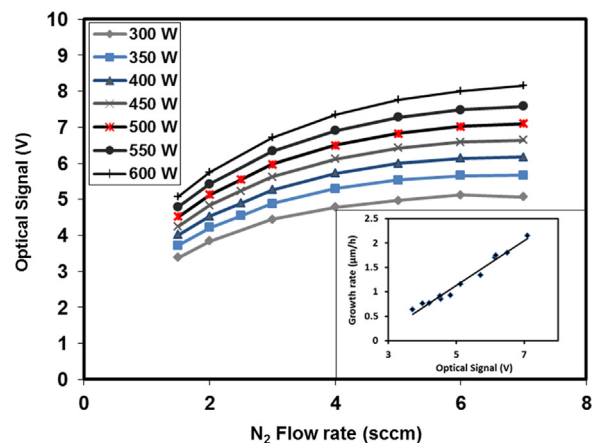


Fig. 2. Intensity of the light emitted by the plasma as a function of N_2 flow rate and HDRS RF power. The inset shows the correlation between the growth rate and the optical signal intensity.

confirmed by the correlation between the growth rate and this signal (inset of Fig. 2). This validates the use of the optical data. More, looking at Fig. 2, one can anticipate that growth rate can be further enhanced beyond 2.3 $\mu\text{m}/\text{h}$ with an RF power of 600 W. For comparison, we remind that maximum growth rates of 2.2 $\mu\text{m}/\text{h}$ and 2.65 $\mu\text{m}/\text{h}$ have been achieved using powers of 500 W and 600 W respectively with another high density plasma source technology [3]. FTIR measurements have been performed on 0.5–2.2 μm thick GaN films grown on 3 in. diameter AlN/Si(111) templates. Thickness variation $(h_{\text{max}} - h_{\text{min}})/h_{\text{max}}$ of GaN over 30 mm from the center toward the edges is slightly better with the HDRS (6.5%) compared with the CS source (8.8%).

3.2. GaN layers quality

Despite the huge increase in growth rate, RHEED attests for a smooth surface and this is confirmed by AFM. Fig. 3 shows a $2 \times 2 \mu\text{m}^2$ scan of the surface of a 2 μm thick GaN film grown at 2.1 $\mu\text{m}/\text{h}$ on a GaN-on-Sapphire template (RF power of 500 W, N_2 flow rate of 7 sccm). One clearly sees the features revealing the spiral growth around a dislocation with a screw-component [13]. The profile of heights along the line drawn on this figure reveals the presence of ~ 0.25 nm height steps that we can attribute to single molecular monolayer steps. The root mean square (RMS) roughness in this area is 0.5 nm. Larger area scans reveal an increase of the roughness which can reach 2.3 nm for $10 \times 10 \mu\text{m}^2$ due to the combination of the initial large range roughness of the

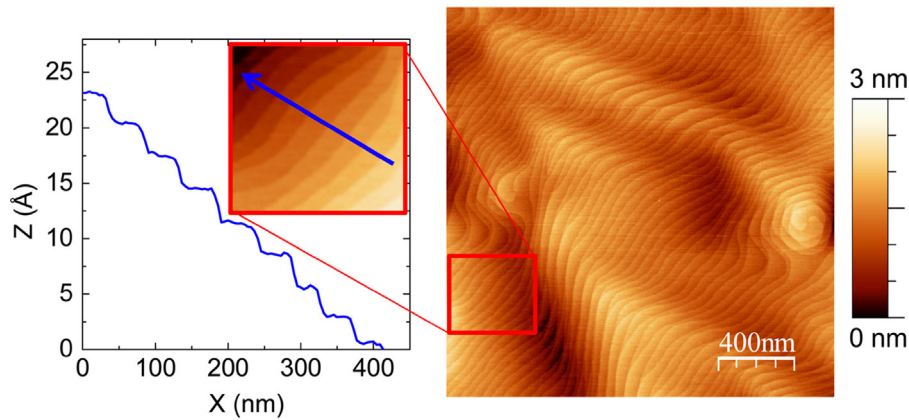


Fig. 3. AFM surface morphology of a 2 μm thick GaN film grown at 2 $\mu\text{m}/\text{h}$ and height profile along the line drawn on the left picture using WSxM software [14].

Table 1

Growth conditions, resulting growth rates and concentrations of impurities measured by SIMS in GaN films grown with the CS and the HDRS cells.

Sample	Sample	Growth rate ($\mu\text{m}/\text{h}$)	Silicon (at/cm^3)	Oxygen (at/cm^3)	Carbon (at/cm^3)	Boron (at/cm^3)
GaN1	Template 1		4×10^{15}	1×10^{17}	$6\text{--}9 \times 10^{16}$	
	CS 400 W 1.8 sccm	0.43 [7]	$4\text{--}5 \times 10^{16}$ [7]	$1\text{--}2 \times 10^{17}$ [7]	8×10^{16} [7]	
GaN2	Template 2		$2\text{--}3 \times 10^{18}$	1×10^{17}	$6\text{--}7 \times 10^{16}$	
	HDRS 400 W 1 sccm	0.53	8×10^{15}	3×10^{17}	7×10^{16}	5×10^{18}
	HDRS 400 W 3.5 sccm	1.15	6×10^{15}	2×10^{17}	5×10^{16}	2×10^{18}
	HDRS 500 W 3.5 sccm	1.28	8×10^{15}	3×10^{17}	6×10^{16}	3×10^{18}
GaN3	HDRS 400 W 4 sccm	1.2	10^{16}	2×10^{17}	5×10^{16}	1.5×10^{18}
	HDRS 500 W 7 sccm	2.1	$2\text{--}3 \times 10^{15}$	$3\text{--}5 \times 10^{17}$	$8\text{--}10 \times 10^{16}$	2×10^{18}
NH ₃	NH ₃ 200 sccm	0.6	$1\text{--}2 \times 10^{15}$	$1\text{--}2 \times 10^{17}$	5×10^{16}	

template and the MBE growth process. In conclusion, in spite of the low temperature (720 $^{\circ}\text{C}$) compared to MOVPE (> 1000 $^{\circ}\text{C}$), the HDRS is efficient enough to obtain a similar growth rate without a dramatic increase of the roughness, thanks to the enhanced adatom mobility in presence of a Ga-bilayer at the growing surface.

Secondary ion mass spectrometry is used to determine the concentrations of impurities in the grown films. The comparison of GaN films grown on GaN-on-sapphire MOVPE templates is shown in Table 1. The first sample (GaN1) has been grown previously with a CS source and the same gas installation. Data are taken from [7]. The second sample (GaN2) consists of 4 GaN layers each with thicknesses of ~ 0.4 μm grown with the HDRS at various RF powers and N₂ flow rates (400–500 W, 1–4 sccm) with resulting growth rates ranging from 0.5 to 1.28 $\mu\text{m}/\text{h}$. These layers have been grown on a GaN-on-sapphire MOVPE template intentionally doped with silicon at $2\text{--}3 \times 10^{18}/\text{cm}^3$ (labeled Template 2 in Table 1). The third sample (GaN3) is the previously mentioned 2 μm thick GaN layer grown at 2.1 $\mu\text{m}/\text{h}$ with the HDRS and the last sample is the same structure grown at 0.6 $\mu\text{m}/\text{h}$ by NH₃ MBE. Compared with our previous works with a CS source [7], the silicon concentration ($6\text{--}10 \times 10^{15}/\text{cm}^3$) is clearly lowered. Note that in Template 1 and Template 2 the levels of Oxygen and Carbon are similar. Carbon levels in GaN grown with both sources are as low as in the templates, but progresses still have to be made in terms of Oxygen concentration. The differences between the HDRS and the CS cells persist for similar growth rates leading to a possible origin related to the plasma cells materials. Moreover, this SIMS

analysis has been completed with the tracking for Boron and Iron species. The absence of Iron is good news as Fe atoms induce deep energy levels in GaN. On the other hand, Boron concentrations are in the range of the mid $10^{18}/\text{cm}^3$ which seems sufficiently low to consider GaN as a pure material. Finally, the variation of impurity concentrations with the growth parameters globally confirms a reduction with the increase of the growth rate at a given RF power (400 W in the present case) and a limited increase while changing the RF power to 500 W at nitrogen flow rates of 3.5–4 sccm with growth rates in the same range (1.15–1.28 $\mu\text{m}/\text{h}$). According to capacitance–voltage (CV) measurements, the residual donor density is $(8\text{--}12) \times 10^{16}/\text{cm}^3$ in GaN grown with the HDRS source and in the $(5\text{--}9) \times 10^{16}/\text{cm}^3$ with the CS source [7]. SIMS data indicates that the main impurity is Oxygen, plus Silicon when using the CS with a partial compensation with Carbon acceptors. Both Oxygen and Silicon are shallow donors in GaN which may explain the n type doping revealed by CV measurements. However, the slightly lower doping level obtained with the CS compared with the HDRS is not fully consistent with SIMS data, even when taking into account the Carbon impurities. Nitrogen vacancy is a donor defect in GaN [15] and the slightly larger residual doping in GaN grown at high growth rate may find its origin in the amount of such a kind of defect. On the other hand, as reported in Table 1, NH₃ MBE grown GaN contains similar amounts of Oxygen and Carbon while producing residual donor densities of a few $10^{14}/\text{cm}^3$ [7]. A larger amount of Hydrogen in NH₃ MBE grown GaN may explain this, as Hydrogen can passivate many kinds of defects [16], including the doping impurities.

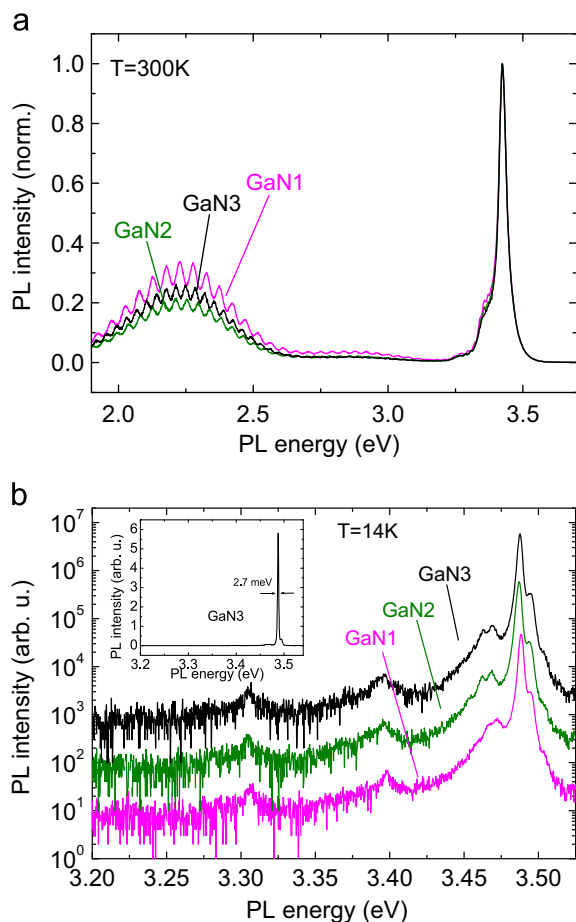


Fig. 4. Photoluminescence spectra of samples GaN1 (conventional source, 400 W/1.8 sccm), GaN2 (HDRS, 400 W/4 sccm), and GaN3 (HDRS 500 W, 7 sccm) at room temperature (a) and low temperature (b). The inset of Fig. 4b corresponds to the low temperature photoluminescence spectrum of sample GaN3 in linear scale.

The optical properties of such GaN films are assessed by room- and low-temperature PL on the 3 samples labeled GaN1, GaN2 and GaN3. The room temperature spectra are dominated by the GaN A-free exciton at 3.425 eV (Fig. 4a). Compared to the integrated PL peak intensity of the GaN band edge of GaN1 (I_{GaN1}), the integrated PL peak intensity is $0.6 \times I_{\text{GaN1}}$ for GaN2 and $0.4 \times I_{\text{GaN1}}$ for GaN3. The larger PL intensity of GaN1 compared to GaN2 and GaN3 could be related to an increase of the point defect density in these samples. However we cannot discard the fact that a higher n-type non intentional doping in sample GaN1 (especially by Si which is a shallow donor in GaN) can be at the origin of its higher PL intensity compared to samples GaN2 and GaN3 [17]. A broad band, structured by interference fringes, is centered at 2.24 eV. This band is commonly designed as the “yellow band” and is typical of deep level emission in GaN. The origin of this band is object of debate. It has been first proposed that it was related to the presence of Ga-vacancies [18] before that Carbon (C_N , or $C_N O_N$ complex) was proposed as the main responsible for this luminescence [19]. In principle, the intensity ratio between the band-edge emission and the deep yellow band emission can give an idea of the GaN material quality. However, in such structures regrown on GaN-on-Sapphire templates, yellow PL may originate from the MOVPE-template. While direct excitation of the template by the laser can be excluded when the MBE-grown layer exceeds a thickness of about 100 nm, the PL of the MBE-grown layer can excite the template indirectly. For this reason, it remains difficult to draw any conclusion on yellow PL. The low temperature PL spectra of the same samples near the band-edge of GaN are shown

in Fig. 4b. All the spectra are dominated by the neutral donor-bound exciton I_2 at energy of 3.487 eV. We remind that according to SIMS measurements, a high concentration of Oxygen is found in all the samples. Therefore, Oxygen is probably the main impurity involved in this I_2 peak. Note that the full width at half-maximum (FWHM) of this peak is below 3 meV for the three PAMBE grown GaN samples. It is as narrow as 2.7 meV for sample GaN3 (inset of Fig. 4) indicating that the crystalline quality the GaN-on-sapphire template is not altered during the MBE of GaN at high growth rate ($\sim 2 \mu\text{m/h}$). For comparison a FWHM of 2.4 meV has been obtained at 10 K for the I_2 line of a GaN structure grown by NH_3 MBE [5]. The slightly lower temperature as well as a smaller amount of donor impurities may account for this difference. No donor-acceptor pair luminescence can be detected. This shows that the residual acceptor concentration in these samples is very low. Finally, we can say that the overall properties of the spectra of samples GaN1, GaN2 and GaN3 are very similar and therefore the use of a HDRS at high growth rate can be beneficial to reduce the process time without compromising on the optical quality of the GaN layers.

Positron annihilation spectroscopy was used to study the presence of cation vacancy and cation vacancy-complex defects in the samples with a variable energy positron beam ($E=0\text{--}25 \text{ keV}$). The probed depth increases with the positron energy: at 25 keV the positron mean implantation depth is about $1.2 \mu\text{m}$ in GaN. The trapping of positrons at vacancy defects can be observed as the narrowing of the Doppler-broadened 511 keV annihilation line, recorded with a Ge detector. The measured spectra were characterized by the conventional line shape parameters S and W , determined as fractions of positrons annihilating with low ($|p_{\text{D}}| < 0.4 \text{ a.u.}$) and high momentum electrons ($1.5 \text{ a.u.} < |p_{\text{D}}| < 3.9 \text{ a.u.}$), respectively [12]. Fig. 5a shows the S and W parameters extracted for a reference Mg-doped MBE GaN layer, the previously investigated samples GaN1, GaN2 and GaN3 and a GaN NH_3 MBE grown sample. The Mg-doped (and p-type) MBE GaN is used as a reference as the concentration of vacancy defects to which positron are sensitive has been shown to be below the detection limit of the method in this sample [20], and hence the positron annihilation parameters correspond to those of the GaN lattice. All the curves exhibit two distinct behaviors: a decrease for positron energy inferior to 12 keV then a plateau. At low energy, the positrons annihilate in the near surface region and in the surface states in a proportion decreasing when the energy increases. At higher energy, the plateau shape indicates that the positrons annihilate only in the layer region that appears homogeneous in all samples.

The normalized layer-specific positron annihilation characteristics for all the studied samples are shown in Fig. 5b. The S and W parameters are normalized using the reference sample values ($S_{\text{Ref}}=0.457$, $W_{\text{Ref}}=0.049$). Two reference points corresponding to the gallium vacancy and to a typical in-grown gallium vacancy-related complex are also shown [21]. The annihilation characteristics determined for the NH_3 MBE sample are very similar to those of the reference, meaning that the vacancy-defect concentration is close to the detection limit of the experiment at room temperature, i.e. $\sim 10^{16} \text{ cm}^{-3}$. The (S, W) points relative to the samples GaN1, GaN2 and GaN3 fall on the line pointing to the in-grown V_{Ga} -complex defect highlighting the presence of this kind of defect in the probed layers. The defect concentration can be estimated assuming $S(V_{\text{Ga-complex}})/S_{\text{Ref}}=1.05$ and using a trapping coefficient of $\mu_{\text{v}}=3 \times 10^{15} \text{ s}^{-1}$. The obtained concentrations range from $4 \times 10^{16} \text{ cm}^{-3}$ for GaN1 to $2 \times 10^{17} \text{ cm}^{-3}$ for GaN2, as shown in Fig. 5b. The lowest point defect concentrations obtained in GaN1 ($4 \times 10^{16} \text{ cm}^{-3}$) and GaN3 ($6 \times 10^{16} \text{ cm}^{-3}$) are in the same range as the ones reported by Koblmüller on GaN grown by PAMBE at low growth rate under various conditions (temperature, Ga/N flux ratio) on similar crystal quality templates [22]. As GaN1 and GaN3

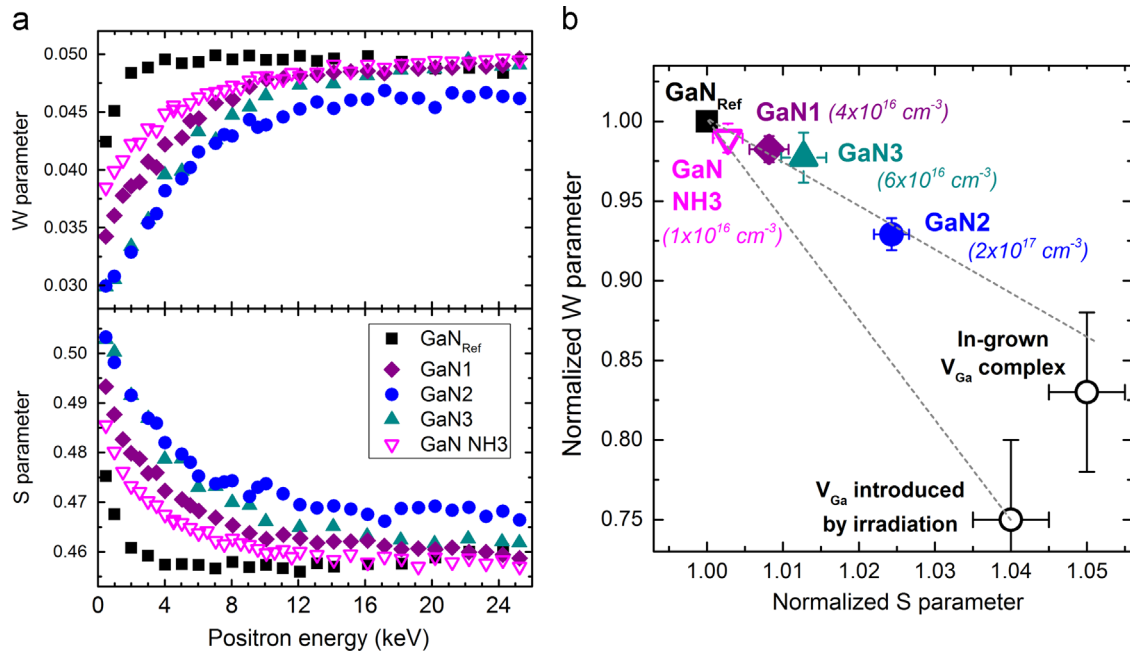


Fig. 5. (a) S and W parameter as function of positron energy for the four MBE grown samples and for a p-type GaN reference. (b) Average S and W normalized parameters for the studied samples. The average values are calculated on the energy range [12–25 keV] corresponding to the layers. The (S, W) parameters characteristic of V_{Ga} and in-grown V_{Ga}-complex are also indicated. The defect concentration estimations are given in brackets.

have been grown at the lowest and the highest rate, respectively, no direct link between the growth rate and the vacancy generation can be deduced from the results. Whatever the mechanisms involved it appears from Fig. 5 that the sample GaN3 grown at a noticeably higher growth rate (higher power and larger nitrogen flow rate) is still close to the reference in terms of point defects.

3.3. GaN/AlGa_N quantum wells

An efficient plasma source is useful for growing thick structures in a reduced time. In order to evaluate the impact of the buffer growth rate on the quality of GaN/AlGa_N quantum wells (QW), two identical structures with 30 nm (top) and 50 nm (bottom) Al_{0.12}Ga_{0.88}N barriers and 3 nm GaN wells have been grown with 0.5–0.8 μm thick buffer layers on 3–4 μm GaN-on-sapphire templates. In structure QW1, both the GaN buffer layer and the GaN/AlGa_N active region have been grown at 0.5 μm/h (400 W/1 sccm). In structure QW2, the GaN buffer growth rate has been increased to 1.7 μm/h (400 W/6 sccm) while the rest of the layers is grown as previously. For this purpose, a second Ga effusion cell was used to obtain the required flux for an optimal quality at high growth rate. Fig. 6 shows the cross section TEM view of the structure QW2 on the GaN buffer grown at high growth rate. One can notice the well-defined flat interfaces. The thickness of the GaN quantum well is estimated to 3.5 nm.

Fig. 7 shows the room temperature PL spectra of samples QW1 and QW2. The PL spectra present very similar features. The spectra are largely dominated by the fundamental e₁–hh₁ transition of the GaN/AlGa_N QW (3.456 eV and 3.453 eV for samples QW1 and QW2, respectively). As illustrated in the inset of Fig. 7, these energy values are higher than that of the GaN buffer layer (3.425 eV) and this attests of carrier confinement in the GaN QW. Note that the QW thickness is too thin to induce a quantum confined Stark effect sufficient to obtain transition energy below the bandgap of GaN [23,24]. A high energy peak coming from the AlGa_N barrier layer is observed at 3.665 eV for sample QW1 and 3.664 eV for sample QW2. The FWHM of the peaks corresponding to the QW emission of sample QW1 and QW2 are 86 meV and 77 meV, respectively. From the X-ray

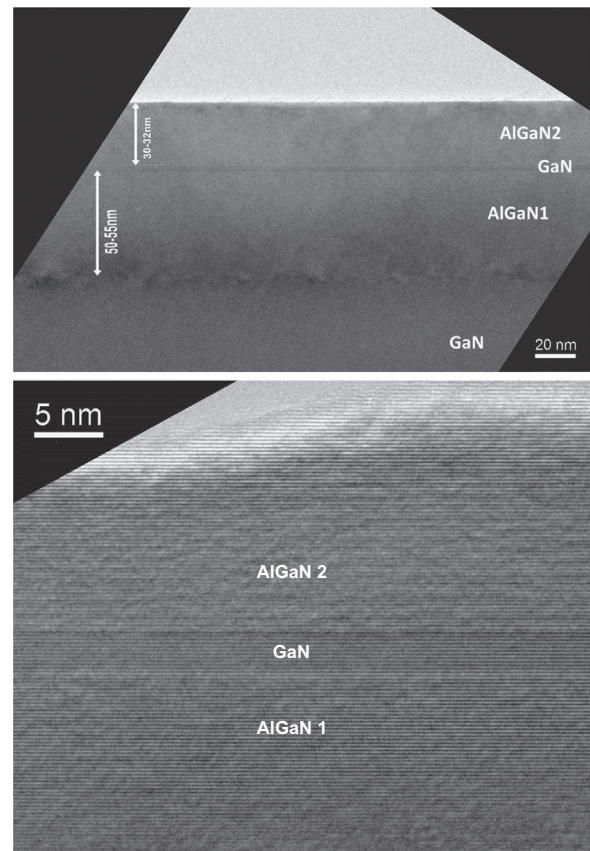


Fig. 6. Cross section transmission electron microscopy views along the [14–50] zone axis of the AlGa_N/GaN quantum well structure QW2 on a GaN buffer grown at 1.7 μm/h.

measurements we deduced Al contents of 12% and 11.8% in the AlGa_N barriers of samples QW1 and QW2 respectively. For both samples, the QW fundamental transition and the barrier PL energy values are very close. This indicates that we have good control of the

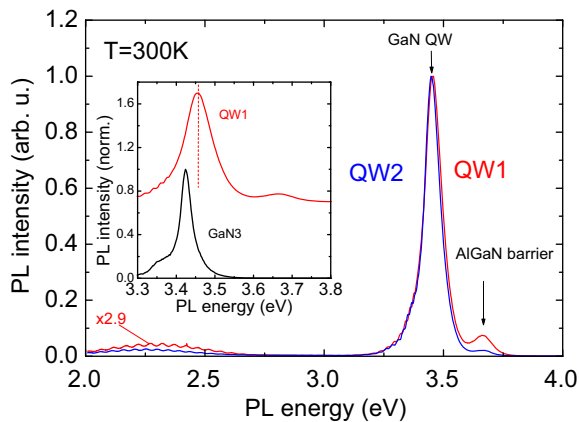


Fig. 7. Room temperature photoluminescence (PL) spectra of GaN/AlGaIn quantum wells grown using the HDRS. The GaN buffer layer growth rates are 0.5 $\mu\text{m}/\text{h}$ and 1.7 $\mu\text{m}/\text{h}$ for samples QW1 and QW2, respectively. The inset shows the high energy part of the room temperature PL spectrum of sample QW1 compared to that of simple GaN layer (sample GaN3).

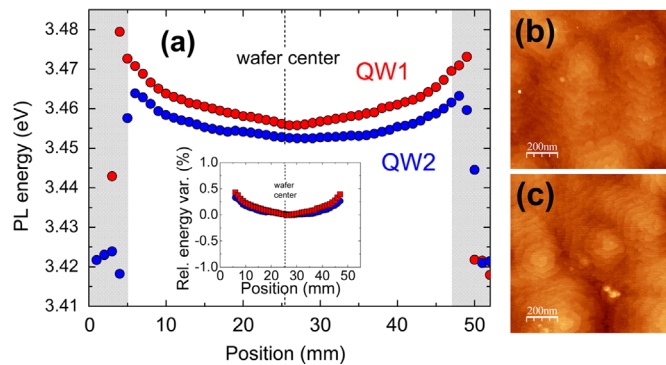


Fig. 8. (a) Variation of the fundamental e1-hh1 photoluminescence energy of GaN/AlGaIn quantum well. The inset corresponds to the relative energy variation using the center of the wafer as the reference. Also presented are the AFM images of the surface of QW2 sample (b) at the center and (c) at 20 mm from the center.

GaN QW thickness and the Al composition of the AlGaIn layers using the HDRS. We remark that the peak PL intensity of sample QW2 is nearly 3 times larger than that of sample QW1. This proves that using large growth rate for the GaN buffer layer (1.7 $\mu\text{m}/\text{h}$ for sample QW2) has no negative impact on the QW internal quantum efficiency.

The analysis reported above concerns the center of the wafers. In order to get information about the sample uniformity with the HDRS, we have mapped the PL along the wafer diameter. The diameter is 2 in. The energy corresponding to the QW fundamental transition energy is reported as a function of the position on the wafer diameter in Fig. 8. A 5 mm exclusion zone accounts for the combination of two effects already observed with our MBE system [5,8]: the shadowing effect of the molybdenum substrate holder and the temperature variation that can degrade the layer quality. The PL energy is quasi constant up to a distance of 10 mm away from the wafer center. There is a trend to an increase of the energy at the wafer edges. The increase is of 10–15 meV over 20 mm from the center while it was 35–40 meV with QWs grown with the CS [8]. This better uniformity (4% on GaN QW thickness over 20 mm) is consistent with the abovementioned enhanced thickness uniformity and results in a relative energy variation below 0.5%. AFM measurements performed at the center and 20 mm away from the center show that the surface morphology of the QW structure and its roughness are not changed (RMS=0.5 nm on $1 \times 1 \mu\text{m}^2$ area). This indicates that over a distance of 20 mm from the center of the wafer, the growth

conditions are not sufficiently altered to modify the layer quality, at least for this kind of structure.

4. Conclusions

In the present work the plasma assisted MBE growth of GaN and AlGaIn compounds with a high density radical source (HDRS) has been studied. The high efficiency in terms of production of active nitrogen species is verified and allows reaching growth rates noticeably larger than those obtained with a conventional source (CS). Not only growth rates superior to 2 $\mu\text{m}/\text{h}$ can be obtained using an RF power of 500 W and a nitrogen flow rate of 7 sccm, but growth at 1 $\mu\text{m}/\text{h}$ is easily achieved with quite standard conditions (400 W, 2 sccm nitrogen flow rate). The structural and optical characterizations of GaN films do not exhibit noticeable differences in quality compared with materials grown at lower growth rate. This is also the case of GaN/AlGaIn quantum wells grown using identical conditions on buffer layers obtained at growth rates of 0.5 $\mu\text{m}/\text{h}$ and 1.7 $\mu\text{m}/\text{h}$. More a slight enhancement in uniformity is obtained. The SIMS analysis of the grown GaN layers shows differences in impurity concentrations, especially silicon, depending on the nitrogen source and the plasma conditions. However, the difference between donor and acceptor impurities concentrations does not seem to account for the n-type residual doping of the layers; involving other donor defects like nitrogen vacancies may explain the present results. On the other hand positron annihilation experiments reveal gallium vacancy-related complexes whose density depends on the plasma conditions. An interesting point is that increasing the growth rate from 0.43 $\mu\text{m}/\text{h}$ with a CS to 2.1 $\mu\text{m}/\text{h}$ with an HDRS plasma source enlarged the defect density by $2 \times 10^{16} \text{ cm}^{-3}$ only.

Acknowledgments

The technology facility network RENATECH and the National Research Agency (Grant “Investissements d’Avenir” ANR-11-LABX-0014) are deeply acknowledged.

References

- [1] R. Aidam, E. Diwo, N. Rollbühler, L. Kirste, F. Benkhelifa, *J. Appl. Phys.* 111 (2012) 114516.
- [2] Y. Kawai, S. Chen, Y. Honda, M. Yamaguchi, H. Amano, H. Kondo, M. Hiramatsu, H. Kano, K. Yamakawa, S. Den, M. Hori, *Phys. Status Solidi C* 8 (7–8) (2011) 2089–2091.
- [3] B.M. McSkimming, F. Wu, T. Huault, C. Chaix, J.S. Speck, *J. Crystal Growth* 386 (2014) 168–174.
- [4] S. Chen, Y. Kawai, H. Kondo, K. Ishikawa, K. Takeda, H. Kano, M. Sekine, H. Amano, M. Hori, *Jpn. J. Appl. Phys.* 52 (2013) 021001.
- [5] Y. Cordier, F. Pruvost, F. Semond, J. Massies, M. Leroux, P. Lorenzini, C. Chaix, *Phys. Status Solidi C* 3 (2006) 2325–2328.
- [6] Y. Cordier, F. Semond, J. Massies, M. Leroux, P. Lorenzini, C. Chaix, *J. Crystal Growth* 301–302 (2007) 434–436.
- [7] Y. Cordier, F. Natali, M. Chmielowska, M. Leroux, C. Chaix, P. Bouchaib, *Phys. Status Solidi C* 9 (3–4) (2012) 523–526.
- [8] F. Natali, Y. Cordier, C. Chaix, P. Bouchaib, *J. Crystal Growth* 311 (2009) 2029–2032.
- [9] F. Natali, Y. Cordier, J. Massies, S. Veizan, B. Damilano, M. Leroux, *Phys. Rev. B* 79 (2009) 035328.
- [10] Y. Cordier, M. Portail, M. Chmielowska, Proceedings of the 11th Expert Evaluation & Control of Compound Semiconductor Materials and Technologies (EXMATEC), Porquerolles, May 30–June 1, 2012.
- [11] K. Klosek, M. Sobanska, G. Tchutchulashvili, Z.R. Zytikiewicz, H. Teisseyre, L. Kłopotowski, *Thin Solid Films* 534 (2013) 107–110.
- [12] F. Tuomisto, I. Makkonen, *Rev. Mod. Phys.* 85 (2013) 1583.
- [13] A.R. Smith, V. Ramachandran, R.M. Feenstra, D.W. Greve, M.-S. Shin, M. Skowronski, J. Neugebauer, J.E. Northrup, *J. Vac. Sci. Technol. A* 16 (1998) 1641.
- [14] I. Horcas, R. Fernandez, J.M. Gomez-Rodriguez, J. Colchero, J. Gomez-Herrero, A.M. Baro, *Rev. Sci. Instrum.* 78 (2007) 013705.

- [15] J.I. Pankove, S. Bloom, G. Harbeke, RCA Rev. 36 (1975) 163.
- [16] A. Hierro, S.A. Ringel, M. Hansen, J.S. Speck, U.K. Mishra, S.P. DenBaars, Appl. Phys. Lett. 77 (2000) 1499.
- [17] E.F. Schubert, I.D. Goepfert, W. Grieshaber, J.M. Redwing, Appl. Phys. Lett. 71 (1997) 921.
- [18] M.A. Reshchikov, H. Morkoc, J. Appl. Phys. 97 (2005) 061301.
- [19] M.A. Reshchikov, D.O. Demchenko, A. Usikov, H. Helava, Yu Makarov, Phys. Rev. B 90 (2014) 235203.
- [20] J. Oila, V. Ranki, J. Kivioja, K. Saarinen, P. Hautajarvi, J. Likonen, J. M. Baranowski, K. Pakula, T. Suski, M. Leszczynski, I. Grzegory, Phys. Rev. B 63 (2001) 045205.
- [21] F. Tuomisto, T. Paskova, R. Kroger, S. Figge, D. Hommel, B. Monemar, R. Kersting, Appl. Phys. Lett. 90 (2007) 121915.
- [22] G. Koblmüller, F. Reurings, F. Tuomisto, J. Speck, Appl. Phys. Lett. 97 (2010) 191915.
- [23] N. Grandjean, B. Damilano, S. Dalmaso, M. Leroux, M. Lügt, J. Massies, J. Appl. Phys. 86 (1999) 3714.
- [24] F. Natali, D. Byrne, M. Leroux, B. Damilano, F. Semond, A. Le Louarn, S. Veziar, N. Grandjean, J. Massies, Phys. Rev. B 71 (2005) 075311.